Optical studies of CdSe/HgSe and CdSe/Ag_2Se core/shell nanoparticles embedded in gelatin

2008 J. Phys.: Condens. Matter 20 455203

(http://iopscience.iop.org/0953-8984/20/45/455203)

J. Phys.: Condens. Matter **20** (2008) 455203 (9pp) doi:10.1088/0953-8984/20/45/455203

Optical studies of CdSe/HgSe and CdSe/Ag_2Se core/shell nanoparticles embedded in gelatin

Yu M Azhniuk[1], V M Dzhagan[2], A E Raevskaya[3], A L Stroyuk[3], S Ya Kuchmiy[3], M Ya Valakh[2] and D R T Zahn[4]

[1] Institute of Electron Physics, Ukrainian National Academy of Sciences, Universytetska Street 21, Uzhhorod 88017, Ukraine
[2] Institute of Semiconductor Physics, Ukrainian National Academy of Sciences, Prospect Nauky 41, Kyiv 03028, Ukraine
[3] Institute of Physical Chemistry, Ukrainian National Academy of Sciences, Prospect Nauky 31, Kyiv 03028, Ukraine
[4] Chemnitz University of Technology, Semiconductor Physics, D-09107 Chemnitz, Germany

E-mail: yu.azhniuk@gmail.com

Received 1 February 2008, in final form 29 August 2008
Published 13 October 2008
Online at stacks.iop.org/JPhysCM/20/455203

Abstract
CdSe/HgSe and CdSe/Ag_2Se core–shell nanoparticles are obtained by colloidal synthesis from aqueous solutions in the presence of gelatin. Optical absorption, luminescence, and Raman spectra of the nanoparticles obtained are measured. The variation of the optical spectra of CdSe/HgSe and CdSe/Ag_2Se core–shell nanoparticles with the shell thickness is discussed. Sharp non-monotonous variation of the photoluminescence spectra at low shell coverage is observed.

(Some figures in this article are in colour only in the electronic version)

1. Introduction

In recent decades core–shell structures based on II–VI semiconductor nanocrystals have become an extensively studied class of nanosystems due to their remarkable luminescence properties leading to numerous applications in nonlinear optics, optoelectronics, and biology [1–5]. A wider-bandgap shell provides the passivation of active surface states of the nanoparticle core and efficient elimination of non-radiative recombination channels. The radiative recombination of the photogenerated excitons in such structures is thus remarkably enhanced (e.g. [6–9]). High luminescence efficiency, broad tunability over the whole visible spectral range and a narrow size distribution within the nanoparticle ensemble are reported for nanostructures, based on a CdSe nanocrystal core and CdS or ZnS shells [6, 7, 10–12]. Many studies, not only of luminescent and absorption properties of CdSe/CdS and CdSe/ZnS core–shell nanostructures, obtained by various techniques, but also of their internal structure by high-resolution transmission electron microscopy, x-ray techniques, resonant Raman scattering and other techniques have been carried out [7–9, 13–24].

For semiconductor nanostructures where the core is surrounded by a shell with narrower bandgap, e.g. HgSe or Ag_2Se, a considerable increase of luminescence efficiency can hardly be expected. On the contrary, one should rather predict its quenching due to the possibility of the photogenerated charge-carrier recombination within a narrower-gap shell. However, studies of such structures seem interesting, not only because they could further expand optical and photochemical applications of II–VI core–shell nanostructures, but also in view of obtaining specific data regarding the formation of core–shell interfaces which can be obtained from the analysis of variation of their optical properties with the effective shell thickness. A comparison of the behaviour of CdSe-based nanostructures obtained by similar techniques with different shell materials can provide additional data on the specific features of shell formation. To our knowledge only one study concerning the optical properties of CdSe/HgSe core–shell

structures has been reported [25] and no studies of CdSe/Ag_2Se nanostructures have been published so far.

Here we report on obtaining CdSe/HgSe and CdSe/Ag_2Se core–shell nanoparticles by colloidal synthesis and their characterization by resonant Raman scattering, optical absorption and photoluminescence spectroscopy.

2. Experimental details

All reagents ($CdSO_4$, Se, Na_2SO_3, $AgNO_3$, $Hg(NO_3)_2$ and gelatin) were obtained from Aldrich and used without additional purification. Sodium selenosulfate (Na_2SeSO_3) solutions were prepared by dissolving selenium powder in a hot (90–95 °C) 0.6 M Na_2SO_3 solution at a molar ratio of [Se]:[Na_2SO_3] = 1:4. Pure selenium was dissolved quantitatively in a solution of pure sodium sulfite. Some further analytical experiments were then performed with the selenosulfate. First, selenium was precipitated from Na_2SeSO_3, dried and its mass measured. The quantity of selenium dissolved was equal to that precipitated. Therefore, no other form of Se than Na_2SeSO_3 (for example, Na_2SeO_2, Na_2SeO_3, etc) was present in the solution. This experiment was repeated with a filter paper soaked with Bi^{III} salt held above the solution. If Se^{2-} was formed, then H_2Se would have been released at an acid (HCl, H_2SO_4) addition and a dark stain of Bi_2Se_3 would have been visible on the filter paper. No dark spots were observed indicating the absence of Se^{2-}. Hence, it was reasonable to conclude that no other forms of selenium, either reduced to Se^{2-}, or oxidized to Se^{4+} or Se^{6+}, except Na_2SeSO_3, were present in the solutions.

Two sets of samples with CdSe/HgSe and CdSe/Ag_2Se core–shell nanoparticles were prepared differing in the size of the cadmium selenide core. In the typical preparation 25 ml 5×10^{-2} M $CdSO_4$ solution containing 5 mass% gelatin was mixed with 25 ml of a solution containing 5×10^{-2} M Na_2SeSO_3, 0.15 M Na_2SO_3 and 5 mass% gelatin at room temperature under vigorous stirring. The mixture was cooled to 8 °C to form a gel and kept at this temperature in the dark for 20 h. Then the gel with CdSe nanoparticles was chopped into small pieces and washed repeatedly with ample amounts of distilled water for 24 h. The resulting purified gel was then heated to 20 °C to become a sol and divided into two volumes, one of which was heated at 96–98 °C for 5 h ('large-core' nanoparticles), while the other was kept untreated ('small-core' nanoparticles). Each volume of the CdSe sol was then mixed with 10 mass% gelatin solution to give 1×10^{-3} M CdSe colloid ('zero-shell' nanoparticles). The details of the procedure and the mechanism of the reaction leading to the formation of CdSe core nanoparticles, are given in our earlier papers [26, 27].

To form a shell on the CdSe nanoparticle core an amount of silver (I) or mercury (II) nitrate was added to the colloidal CdSe solution at 75–80 °C under vigorous stirring. The Ag(I) and Hg(II) ions substituted Cd(II) on the surface of CdSe nanoparticles due to lower solubility of Ag_2Se and HgSe as compared with CdSe. The amount of HgSe was varied from 5 mol% (5×10^{-5} M/1×10^{-3} M CdSe) to 50 mol%, while the amount of Ag_2Se was changed from 2.5 mol% to 30 mol%. These solutions were used for the deposition of the films.

The polymer films were prepared in the following manner. A glass plate (8 cm^2) was cleaned by its consecutive treatment with concentrated hydrogen peroxide and sulfuric acid, then washed with distilled water. 2–2.5 ml of a colloidal solution were deposited at room temperature onto the glass plate and allowed to dry slowly in the dark with mild air circulation for 3–4 days. In this case gelatin plays two roles—as a host matrix incorporating CdSe nanoparticles, and as a stabilizer of the growing nanoparticles in the colloidal solution. The films obtained were 0.20–0.25 mm thick, with good optical quality and remarkable mechanical strength.

Resonant micro-Raman scattering and photoluminescence (PL) measurements were performed using a Dilor XY 800 triple monochromator equipped with a CCD camera. A He–Cd laser (λ_{exc} = 441.6 nm) was used for luminescence excitation and an Ar^+ (λ_{exc} = 488.0 and 514.5 nm) provided Raman excitation. The instrumental resolution of the Raman measurements was 2.5–3 cm^{-1}. Optical absorption spectra were measured using a computer-controlled LOMO MDR-23 monochromator with a step-motor driver, an OP-33-0.3 filament lamp, and a FEU-100 phototube. All measurements were carried out at room temperature.

3. Results and discussion

Optical absorption spectra of initial CdSe nanoparticles embedded in gelatin films are shown by solid lines in figures 1 and 2. The observed confinement-related maxima in the absorption spectra are seen to be quite distinct. Since the earliest studies of the confinement-related effect in the optical spectra of semiconductor nanocrystals there has been an enormous work done on a comparative characterization of semiconductor nanoparticles by direct structural (transmission electron microscopy (TEM), x-ray diffraction) and indirect (optical) methods for the nanoparticles of CdSe and other II–VI semiconductors in various host media (e.g. [1, 2, 28–33] and references therein). As a result, a number of calculated and phenomenological dependences have been obtained, making it possible to derive the average nanoparticle size (and size dispersion in some cases) from the optical spectra (absorption and PL), especially from the energy position E_1 of the first absorption maximum [28, 30, 34–40]. The simplest relationship is given by the effective-mass approximation [34]

$$E_1 = E_b + \frac{2\hbar^2}{d^2}\left[\frac{1}{m_e^*} + \frac{1}{m_h^*}\right], \qquad (1)$$

where E_b is the energy gap of the bulk crystal, d is the nanocrystal diameter, m_e^* and m_h^* are the effective masses of electrons and holes, respectively. This model shows a good agreement with the TEM and x-ray diffraction (XRD) data for d > 4–5 nm, but results in a noticeable deviation for smaller nanocrystals. Therefore, we based our estimations on the phenomenological dependence derived in [38], as it agrees well with the experimental data of many authors obtained from independent TEM and XRD measurements [13, 28, 41–43],

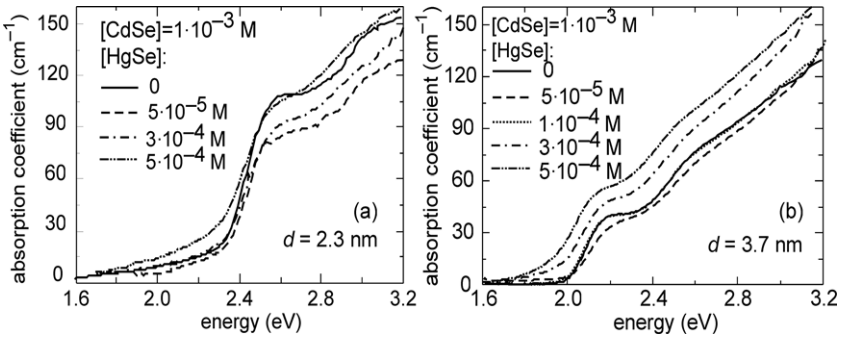

Figure 1. Optical absorption spectra of gelatin-embedded CdSe/HgSe core–shell nanoparticles of the 'small-core' (a) and 'large-core' (b) series. The concentrations of the core and shell compounds in the colloidal synthesis solution, related to the core/shell material ratio in the nanostructures, are indicated in the figure.

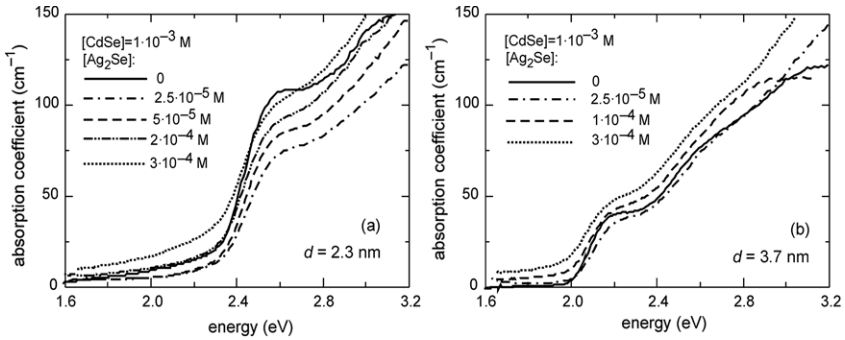

Figure 2. Optical absorption spectra of gelatin-embedded CdSe/Ag_2Se core–shell nanoparticles of the 'small-core' (a) and 'large-core' (b) series. The concentrations of the core and shell compounds in the colloidal synthesis solution, related to the core/shell material ratio in the nanostructures, are indicated in the figure.

as well as with thorough theoretical studies [36]. Our attempts to perform TEM studies of the gelatin-embedded CdSe nanoparticles did not result in good-quality patterns, due to strong charging of the gelatin-stabilized CdSe nanoparticles in the focus of the electron beam and their detachment from the copper grid hindering the obtaining of reliable quantitative information on the size and size distribution of the nanoparticles under consideration. Hence, we relied upon the estimation of the nanoparticle ensemble parameters from the optical absorption spectra which has proven to be fast and reliable. Moreover, while analysing the optical spectra of semiconductor nanocrystals, one can derive collective properties of the whole nanocrystals ensemble, e.g. the average size and the size dispersion, while TEM measurements usually only account for a selected (and very small) area of the sample and may be considered valid only when numerous individual measurements are being made.

Optical absorption spectra of CdSe/HgSe and CdSe/Ag_2Se core–shell nanoparticles embedded in gelatin films are shown in figures 1 and 2. The concentration of the shell compound (HgSe or Ag_2Se) in the colloidal synthesis solution, indicated in the figures, can be considered proportional to the number of shell atoms replacing the core surface atoms and, therefore, can serve as a measure of the effective shell thickness. Taking into account the lattice parameters of CdSe $a = 0.61$ nm (for zinc-blende modification) or $a = 0.43$ nm, $c = 0.70$ nm (for wurtzite modification) [44] and the small size of the CdSe nanocrystals (about 30 unit cells for the 2.3 nm small core and near 120 unit cells for the 3.7 nm large-core nanoparticles), it can be roughly estimated that in the first case nearly 75%, and in the second case almost 50%, of their atoms actually form the nanocrystal surface. Hence, in order to form a one-monolayer (ML) shell one has to substitute at least half of the core atoms. Since in our experiment the shell material concentrations were considerably smaller, we can assume the shell to be non-uniform (island-like or patch-like).

It can also be seen from figures 1(b) and 2(b) that for 3.7 nm CdSe/HgSe and CdSe/Ag_2Se core–shell nanoparticles an increase of the shell effective thickness leads to an increase in the absorption over the whole spectral range and also that the absorption edge together with the confinement-related features shift toward lower energies. Such behaviour has also been observed for different core–shell materials and is usually explained by a partial tunnelling of the core electron wavefunction into the shell [23, 24, 45]. Meanwhile, for the 2.3 nm nanoparticles the shell-induced absorption increase is observed only for energies below the initial onset of CdSe nanoparticle absorption. At higher energies (above E_1) one can instead observe a decrease of the absorption coefficient in the nanoparticles with the lowest effective shell thickness, followed by an increase with further shell formation. Even though this non-monotonous absorption behaviour is seen from figures 1(b) and 2(b) for small-core nanoparticles with both shell types, it can, however, hardly be treated as reliable, since

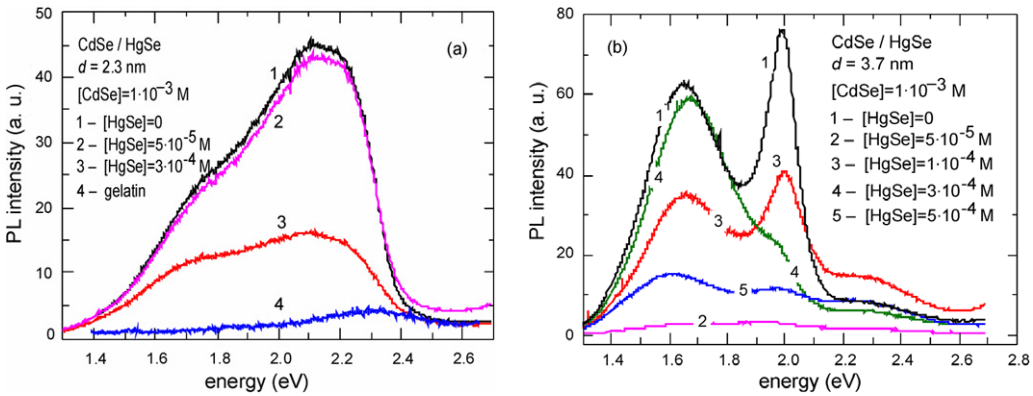

Figure 3. PL spectra of gelatin-embedded CdSe/HgSe core–shell nanoparticles with average core diameter of 2.3 (a) and 3.7 (b) nm as well as the PL spectrum of pure gelatin (curve 4 in (a)). All spectra were measured at room temperature with excitation by the 441.6 nm He–Cd laser line.

we measured the absorption of samples for which no data were available regarding the nanoparticle concentration in the film.

The photoluminescence of CdSe nanoparticles and CdSe-based core–shell structures, which is their most attractive feature from the application point of view, is typically characterized by two bands—a relatively sharp near-bandgap emission peak and a much broader band, significantly shifted towards lower energies, which is attributed to surface-state-mediated recombination [2, 24, 46]. These bands were observed in the PL spectra of the zero-shell CdSe nanoparticles under investigation, shown by curves 1 in figure 3. The near-bandgap band of larger ($d = 3.7$ nm) nanoparticles is considerably narrower. This is possibly related to a narrowing of the size dispersion during the thermal treatment due to Ostwald ripening. The small bandwidth (0.13 eV) of the near-bandgap band for this sample, similarly to the clear first absorption feature in figures 1 and 2, could be the evidence for a relatively narrow size dispersion of CdSe nanoparticles, at least for the sample with $d = 3.7$ nm which, following the discussion in [21, 47], can be estimated as $15 \pm 5\%$. The width of the lower-energy (defect-related) PL band is not representative of the nanoparticle size dispersion. The width of this defect-related band predominantly reflects the distribution of the energy positions of the defect states involved and a strong coupling of the trapped carriers to phonons; this PL band width is similarly large for nanoparticle ensembles with both large and very small size distribution, and very close to the values for bulk crystal [24]. As to the sample with smaller nanoparticles (2.3 nm), the size dispersion is of approximately the same value, as can be supposed from the absorption bandshape being similar to that of the larger nanoparticles. As the PL bandshape is much more sensitive to the surface (defect) structure of the nanoparticles, the large width of the higher-energy PL band in smaller nanoparticles (2.3 nm) is obviously due to the difference in the recombination channels, but not to the size dispersion. For example, new surface-related shallow traps can contribute to this PL band, leading to an apparent broadening of the band.

Contrary to the extensively studied CdSe-based nanoparticles with a wider-bandgap shell (e.g. CdS or ZnS), where a considerable enhancement of the near-bandgap luminescence was observed accompanied with the surface-state-mediated PL band quenching [24], the effect of a narrower-bandgap shell on the PL spectra of the CdSe/HgSe and CdSe/Ag_2Se core–shell nanoparticles under investigation is completely different and essentially depends both on the shell material and the core nanoparticle size. For smaller nanocrystals (figure 3(a)) the increase of HgSe shell effective thickness results in a gradual decrease of both luminescence band intensities. However, for larger nanoparticles (figure 3(b)), the behaviour of the PL band intensities versus the HgSe shell thickness is non-monotonous. The samples with nanoparticles formed in the solution with $[HgSe] = 5 \times 10^{-5}$ M (roughly corresponding to an effective shell thickness of 0.1 ML), exhibit a sharp decrease of both PL band intensities (curve 2 in figure 3(a)). The increase of HgSe concentration to 1×10^4 M, however, partly restores the initial PL band intensities (curve 3). With further shell building, the near-bandgap luminescence band (2.0 eV) intensity gradually decreases while the surface-mediated band (1.7 eV) intensity still continues to increase, almost reaching its initial value at $[HgSe] = 3 \times 10^{-4}$ M (roughly 0.6 ML) before gradually decreasing (figure 3(b)). This non-monotonous behaviour of the PL band intensities is illustrated by figure 4.

The sharp decrease of both PL band intensities at very low HgSe shell effective thickness, observed for the 3.7 nm nanoparticles, can be explained by the fact that at such low Hg concentrations it is more appropriate to consider not the formation of HgSe shell or isolated surface islands, but doping of the CdSe nanocrystal with single Hg atoms. These atoms, located on the nanoparticle surface, act as impurities (mostly isolated, or less probably, due to their small amount in a nanoparticle, small clusters) and result in a considerable number of non-radiative recombination centres which rapidly quench both radiative recombination channels. A further increase in the amount of Hg atoms results in the formation of the HgSe shell (first island-like or patch-like, then with higher coverage). This rearrangement of Hg atoms results in a decrease in the concentration of the non-radiative recombination centres leading to the PL recovery. The general trend of subsequent luminescence quenching with the increase of the shell effective thickness can then easily be explained by the formation of a type-I heterostructure where the conditions

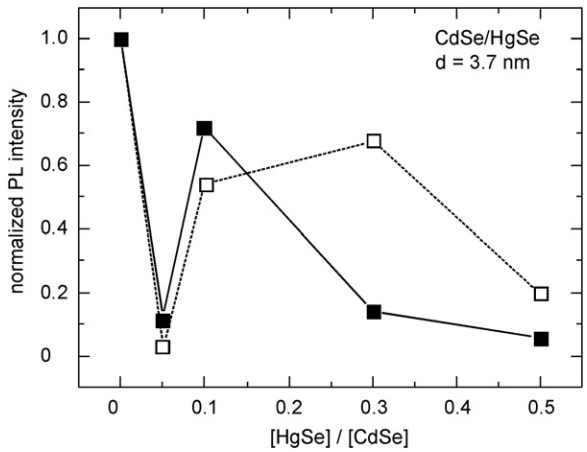

Figure 4. Dependence of the near-edge (2.00 eV, dark squares) and surface-mediated (1.65 eV, open squares) PL band intensities of the gelatin-embedded CdSe/Ag_2Se core–shell nanoparticles with average core size of 3.7 nm on the shell-to-core ratio of the corresponding compound concentrations in the synthesis solution. The PL intensities are normalized by the corresponding band intensity for the zero-shell CdSe nanoparticles. The lines are drawn as guides to the eye.

for exciton recombination in the narrower-gap shell are much more favourable.

The gradual decrease of PL in smaller-core (2.3 nm) CdSe/HgSe core–shell structures, without a sharp drop of intensity at very low Hg amounts (figure 3(a)), is evidently related to the fact that, due to the much smaller nanoparticle surface, the smallest concentration of HgSe (5×10^5 M) corresponds to shell coverages of about three times more in this case than for the 3.7 nm nanoparticles, and, accordingly, one should consider the formation of at least a patch-like shell rather than isolated impurity atoms.

It should also be noted that the authors of the only (to our knowledge) paper, devoted to the luminescence of CdSe/HgSe core–shell nanostructures, report a rather different PL behaviour with the shell effective thickness [25]. Similarly to our results, they observed a rapid quenching of the near-bandgap PL band on building up the HgSe shell. However, the intensity of the surface-mediated luminescence band at 1.7–1.8 eV in [25] increases with the shell thickness, contrary to our case. Since the PL band in question is related to CdSe surface states, such a difference can be explained by a strong dependence of the behaviour of CdSe nanoparticle surface states and CdSe/HgSe interface formation on the nanoparticle surface doping procedure, which is different in [25] and in our study.

It should further be noted that a luminescence feature at 2.3 eV observed in the spectra of the 3.7 nm nanoparticles (figure 3(b)), is related to the gelatin matrix luminescence since it is observed in the pure (nanoparticle-free) gelatin films. In the samples with 2.3 nm nanoparticles (figure 3(a)) this band is masked by the more intense near-bandgap PL band of CdSe nanoparticles. Curve 4 in figure 3(a) shows, for comparison, the PL spectrum of pure gelatin without nanocrystals, normalized to the same intensity scale.

Quite different, though also non-monotonous, is the luminescence behaviour of CdSe/Ag_2Se core–shell nanoparticles. Its dependence on the shell thickness also appears to be size-dependent, as can be seen from figure 5.

For the smaller-core (2.3 nm) CdSe/Ag_2Se nanoparticles with a small amount of Ag atoms added ([Ag_2Se] $= 5 \times 10^5$ M) a sharp quenching of the near-bandgap (2.2 eV) PL band is observed along with a drastic increase of the surface-mediated PL band at 1.8 eV (curve 3 in figure 5(a)). Such behaviour can be explained by the introduction of an additional efficient channel of radiative recombination related to Ag atoms acting most likely as acceptors in CdSe. However, in this case one can hardly explain the curve 2 spectrum in figure 5(a), corresponding to the lowest concentration of silver atoms ([Ag_2Se] $= 2.5 \times 10^5$ M). Its shape is not at all intermediate between the zero-shell CdSe (curve 1) and CdSe/Ag_2Se with [Ag_2Se] $= 5 \times 10^5$ M (curve 3), as one would expect from the above speculations, but just exhibits a decrease of both band intensities in comparison with the initial CdSe nanoparticles. In order to elucidate this rather unusual non-monotonous behaviour of CdSe/Ag_2Se core–shell nanoparticles at low shell coverages a more detailed study with a broader range of core sizes and shell effective thicknesses is required. A further increase of the Ag_2Se shell effective thickness is accompanied by a monotonous decrease of both PL bands.

The luminescence of CdSe/Ag_2Se nanoparticles with a 3.7 nm core is characterized by monotonous quenching of both

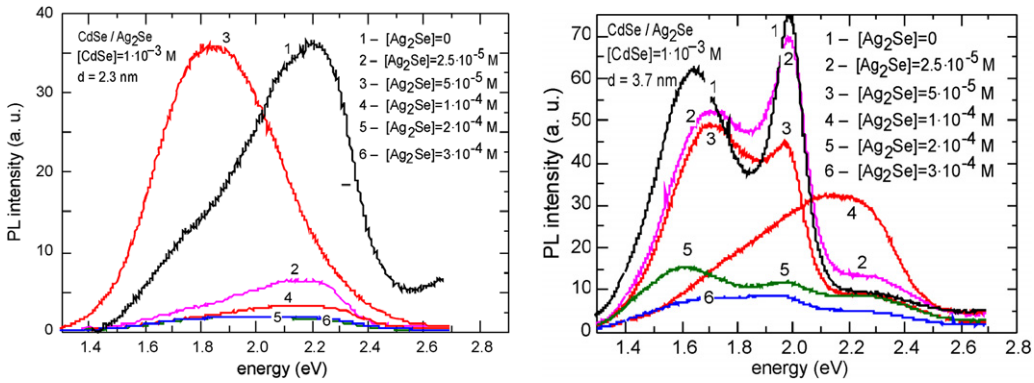

Figure 5. Photoluminescence spectra of gelatin-embedded CdSe/Ag_2Se core–shell nanoparticles with an average core diameter of 2.3 (a) and 3.7 (b) nm, measured at room temperature with excitation by the 441.6 nm He–Cd laser line.

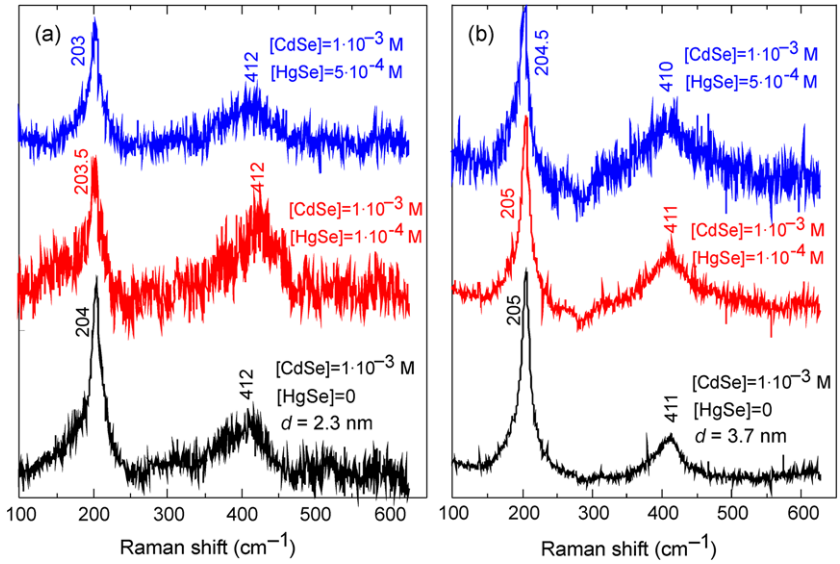

Figure 6. Micro-Raman spectra of gelatin-embedded CdSe/HgSe core–shell nanoparticles with average core diameter of 2.3 (a) and 3.7 (b) nm, measured at room temperature with excitation by the 514.5 nm Ar^+ laser line.

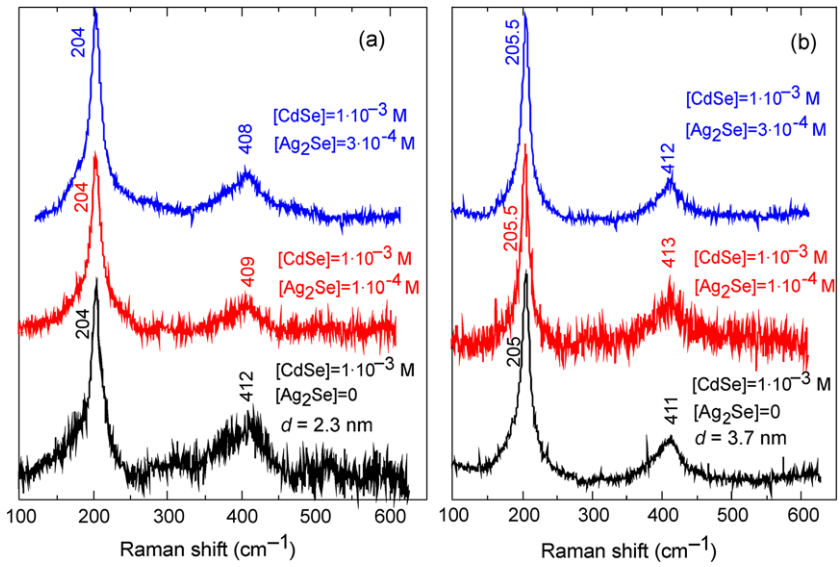

Figure 7. Micro-Raman spectra of gelatin-embedded CdSe/Ag_2Se core–shell nanoparticles with average core diameter of 2.3 (a) and 3.7 (b) nm, measured at room temperature with excitation by the 514.5 nm Ar^+ laser line.

bands on building up the Ag_2Se shell (figure 5(b)). This can be related to much more energetically favourable conditions for exciton recombination in the narrower-bandgap shell.

Note that non-monotonous behaviour of the near-bandgap luminescence with shell thickness was reported earlier for CdSe-based core–shell nanostructures with a wider-bandgap shell, where after reaching a maximum value it decreased with further shell growth. This was explained by shell structure faults caused by lattice misfit-induced strain [6, 7, 9, 48]. In our case, however, the non-monotonous character of PL intensity dependence versus shell thickness is completely different due to the narrow-bandgap shell.

Resonant micro-Raman spectra of CdSe/HgSe and CdSe/Ag_2Se core–shell nanoparticles embedded in gelatin films are shown in figures 6 and 7, respectively. All the spectra contain an LO phonon band at 203–205 cm^{-1} with full width at half maximum (FWHM) of 15–20 cm^{-1} and a two-phonon 2LO band at 408–412 cm^{-1} with FWHM of 60–120 cm^{-1}. It can clearly be seen that the observed LO phonon frequency is lower for smaller nanoparticles (figures 6(a) and 7(a)) than for the larger ones (figures 6(b) and 7(b)) and lower than the value for bulk CdSe (208–210 cm^{-1}) [49, 50]. In the measurements performed for pure gelatin no Raman signal (at least at the excitation with 488 or 514.5 nm laser light) was detected, hence it is clear that the discussed Raman spectra result solely from the nanocrystals.

As regards the possibility of the variation of the lattice parameter in CdSe nanocrystals with respect to the bulk crystal

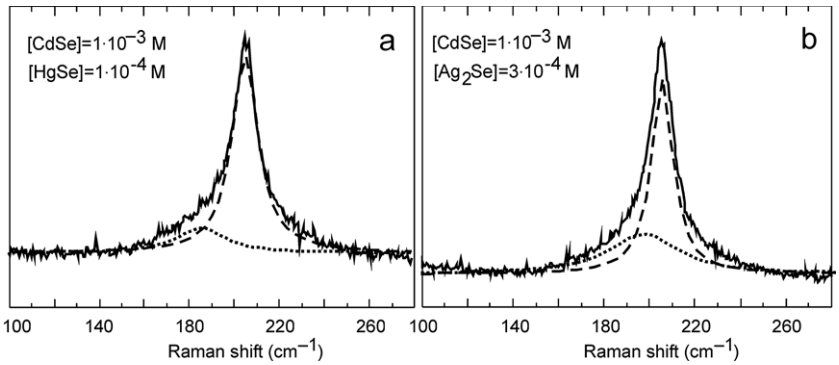

Figure 8. Measured micro-Raman spectra (solid line) of gelatin-embedded CdSe/HgSe (a) and CdSe/Ag_2Se (b) core–shell nanoparticles with an average core radius of 3.7 nm, and their decomposition into the contributions of CdSe core-related LO (dashed line) and surface (dotted line) phonons. The concentrations of the core and shell compounds in the colloidal synthesis solution, related to the core/shell material ratio in the nanostructures, are indicated in the figure.

value, the Raman data (difference in the LO phonon peak frequencies for the bulk and nanometric crystals) show that this variation, if even present, is tiny and its possible effect on the above tentative estimations of the number of unit cells in a nanocrystal is much smaller than other errors arising from the nanocrystal size distribution, non-uniform shell effect, etc.

One of the main factors, responsible for the observed LO phonon frequency decrease with size reduction, is the contribution of non-zero wavevector phonons due to Raman selection rule relaxation caused by phonon confinement in a small nanocrystal volume [51–57]. The phonon confinement results not only in the observed LO phonon frequency decrease, but also in a lineshape asymmetry with a more pronounced lower-frequency wing.

Another important factor, responsible for the observed Raman band asymmetry in nanocrystals, is scattering by surface phonons, with an intensity increasing due to the high surface-to-volume ratio of the nanoparticles [52–59]. The surface phonon frequency is between the TO and LO phonon frequencies. A typical deconvolution of the experimentally measured Raman spectrum of CdSe/HgSe and CdSe/Ag_2Se core–shell nanoparticles is shown in figure 8. The observed CdSe core-related surface phonon frequency (180–190 cm^{-1}) is in agreement with the value reported for CdSe nanocrystals in various media [57, 60, 61] as well as for CdSe/CdS and CdSe/ZnS nanostructures [9, 18, 19, 21, 22]. The detailed comparison of surface phonon behaviour in CdSe-based core–shell nanostructures with different shells will be discussed elsewhere.

The broader 2LO phonon band with a frequency being equal or even somewhat higher than the doubled LO phonon frequency shows that the major contribution to the second-order Raman scattering results from the zone-centre phonons. This is rather typical for II–VI quantum dots [62]. It should also be noted that the parameters of the nanoparticle core-related CdSe LO phonon band (frequency, bandwidth, intensity) are almost independent of the effective thickness of the HgSe or Ag_2Se shell (figures 7 and 8). The very slight decrease of the core CdSe LO phonon frequency with an increase of the effective shell thickness can be related to the core size reduction due to the partial Cd $\rightarrow$ Hg cation substitution in the course of the shell formation.

The number of studies devoted to phonon spectra of core–shell CdSe-based nanostructures, is rather low [9, 18–22], especially in comparison with the studies of their electronic structure. In all cases the core-related CdSe phonon band was observed, its position and shape being analysed with the account of phonon confinement and surface phonon scattering. Note that in CdSe/CdS and CdSe/ZnS nanoparticles, formation of the core/shell structure was accompanied by a narrowing of the CdSe core phonon peak, attributed to an increased lifetime of the optical phonon, confined within the CdSe core, after forming a solid interface with CdS or ZnS [21, 63]. Contrary to the case of CdS or ZnS shells, formed by deposition onto the CdSe nanoparticle surface, here we deal with shells formed by substitution of surface cations. This has obviously less effect on the surface-related broadening of the phonon peak. The present results agree with the idea of the core phonon peak narrowing observed in CdSe/ZnS and CdSe/CdS [21] being related to changes in the vibrational properties of the nanoparticles upon passivation. However, an alternative (or additional) effect of narrowing of the electronic states, mediating the resonant Raman scattering process [60], upon passivation cannot be excluded. The formation of a CdS or ZnS shell also leads to a narrowing of the excitonic PL bands [24].

For CdSe/CdS [18, 19, 21, 22] and CdSe/ZnS [9, 21] core–shell structures the observation of shell-related phonons at a frequency somewhat below the corresponding value for the bulk LO phonon of the shell material has been reported. However, in our case no shell-related phonon bands are observed either for HgSe, or for Ag_2Se shell coated CdSe nanoparticles. This can be explained by several factors. First of all, for both HgSe and Ag_2Se the phonon frequencies are below the core CdSe LO phonon value and the corresponding bands can overlap with Raman contributions from the confinement-related and core surface phonons. Secondly, since the nanoparticles under investigation are dispersed in the gelatin host matrix in such a way that they comprise below 1% of the sample volume, resonant excitation conditions are required for the Raman signal enhancement. However, the Raman excitation wavelength in our experiment did not match the

conditions required for the narrow-bandgap HgSe and Ag_2Se evidently encumbering the observation of the shell-related phonon bands. Finally, since the shell was not uniform and its effective thickness was often below 1 ML, we do not consider its scattering volume sufficient to produce a detectable Raman signal. For the sake of comparison one should mention that in our earlier Raman study of CdSe/CdS and CdSe/ZnS core–shell nanostructures [21], as well as in other studies where shell-related phonons were observed [18, 19, 22], the shell thicknesses were much higher—from 2 to 5.5 ML. Only the authors of [9] claim the observation of ZnS shell-related phonons in CdSe/ZnS nanostructures for a 0.5-ML thick shell.

4. Conclusions

CdSe/HgSe and CdSe/Ag_2Se core–shell nanostructures were synthesized from aqueous solutions and embedded in a transparent gelatin matrix. CdSe core-related LO and 2LO phonon bands have been clearly observed in the Raman spectra of all samples, the LO phonon lineshape being affected by phonon confinement and surface phonon scattering. No Raman signal from the shell could be registered. This is related to the small shell effective thickness, off-resonance scattering conditions and possible superimposition of the expected shell phonons with core surface phonons in the spectra.

Optical absorption spectra of CdSe/HgSe and CdSe/Ag_2Se core–shell nanoparticles show a slight absorption increase and red shift of the confinement-related maxima with the shell thickness, typical for such structures. Contrary to the wider-bandgap shell CdSe-based nanoparticles, in CdSe/HgSe and CdSe/Ag_2Se the increase of effective shell thickness results in quenching of both near-bandgap and surface state-mediated photoluminescence bands. However, this behaviour is not monotonous: mercury or silver atoms in small concentrations act rather as impurities than as shell-forming atoms. The impurity-related formation of non-radiative (at Hg-doping) or radiative (at Ag-doping) recombination centres is considered to be responsible for the non-monotonous behaviour of the PL band intensities at small ($(2.5–5) \times 10^5$ M) concentration of the shell material in the synthesis solution. The shell formation with a further increase of the corresponding compound concentration results in opening of new recombination channels within the shell, leading to a decrease of both PL bands with HgSe or Ag_2Se shell effective thickness.

Acknowledgments

Yu M Azhniuk is grateful to Deutsche Forschungsgemeinschaft for providing financial support for his research stay at Chemnitz University of Technology where the Raman and photoluminescence studies were carried out. V M Dzhagan is grateful to the Alexander von Humboldt foundation for the support of his research at Chemnitz University of Technology.

References

[1] Nalwa H S (ed) 2002 *Nanostructured Materials and Nanotechnology* (San Diego, CA: Academic)
[2] Schmid G (ed) 2004 *Nanocrystals: From Theory to Application* (Weinheim: Wiley–VCH)
[3] Klingshirn C 2004 *Optical Properties* Part 2 (*Landolt–Börnstein—Group III Condensed Matter* vol 34C2) (Berlin: Springer)
[4] Fu A, Gu W, Larabell C and Alivisatos A P 2005 *Curr. Opin. Neurobiol.* **15** 568
[5] Somers R C, Bawendi M G and Nocera D G 2007 *Chem. Soc. Rev.* **36** 579
[6] Peng X, Schlamp M S, Kadavanich A V and Alivisatos A P 1997 *J. Am. Chem. Soc.* **119** 7019
[7] Li J J, Wang Y A, Guo W, Keay J C, Mishima T D, Johnson M B and Peng X 2003 *J. Am. Chem. Soc.* **125** 12567
[8] Kuno M, Lee J K, Dabbousi B O, Mikulec F V and Bawendi M G 1997 *J. Chem. Phys.* **106** 9869
[9] Baranov A V, Rakovich Y P, Donegan J F, Perova T S, Moore R A, Talapin D V, Rogach A L, Masumoto Y and Nabiev I 2003 *Phys. Rev.* B **68** 165306
[10] Rodriguez-Viejo J, Jensen K F, Matoussi H, Michel J, Dabbousi B O and Bawendi M G 1997 *J. Appl. Phys.* **70** 2132
[11] Lee J, Sundar V C, Heine J R, Bawendi M G and Jensen K F 2000 *Adv. Mater.* **12** 1102
[12] Shim M, Wang C and Guyot-Sionnest P 2001 *J. Phys. Chem.* B **105** 2369
[13] Rodriguez-Viejo J, Matoussi H, Heine J R, Kuno M K, Michel J, Bawendi M G and Jensen K F 2000 *J. Appl. Phys.* **87** 8526
[14] Koberling F, Mews A, Philipp G, Kolb U, Potapova I, Burghard M and Basche T 2002 *Appl. Phys. Lett.* **81** 1116
[15] Valerini D, Creti A, Lomascolo M, Manna L, Cingolani R and Anni M 2005 *Phys. Rev.* B **74** 235409
[16] Le Thomas N, Herz E, Schöps O, Woggon U and Artemyev M V 2005 *Phys. Rev. Lett.* **94** 016803
[17] Fisher B, Caruge J M, Zehnder D and Bawendi M 2005 *Phys. Rev. Lett.* **94** 087403
[18] Singha A, Satpati B, Satyam P V and Roy A 2005 *J. Phys.: Condens. Matter* **17** 5697
[19] Singha A and Roy A 2005 *Rev. Adv. Mater. Sci.* **10** 462
[20] Comas F, Trallero-Giner C, Prado S J, Marques G E and Roca E 2006 *Phys. Status Solidi* b **243** 459
[21] Dzhagan V M, Valakh M Y, Raevskaya A E, Stroyuk A L, Kuchmiy S Y and Zahn D R T 2007 *Nanotechnology* **18** 285701
[22] Lu L, Xu X-L, Liang W-T and Lu H-F 2007 *J. Phys.: Condens. Matter* **19** 406221
[23] Wang Q, Pan D, Jiang S, Ji X, An L and Jiang B 2006 *J. Lumin.* **118** 91
[24] Raevskaya A E, Stroyuk A L, Kuchmiy S Y, Dzhagan V M, Valakh M Y and Zahn D R T 2007 *J. Phys.: Condens. Matter* **19** 386237
[25] Xu L, Chen K, Zhu J, Chen H, Huang H, Xu J and Huang K 2001 *Superlatt. Microstruct.* **29** 67
[26] Raevskaya A E, Stroyuk A L and Kuchmiy S Y 2006 *Colloid Interface Sci.* **302** 133
[27] Raevskaya A E, Stroyuk A L, Kuchmiy S Y, Azhniuk Y M, Dzhagan V M, Yukhymchuk V O and Valakh M Y 2006 *Colloids Surf.* A **290** 304
[28] Gaponenko S V 1998 *Optical Properties of Semiconductor Nanocrystals* (Cambridge: Cambridge University Press)
[29] Norris D J, Efros Al L, Rosen M and Bawendi M G 1996 *Phys. Rev.* B **53** 16347
[30] Woggon U 1997 *Optical Properties of Semiconducting Quantum Dots* (Berlin: Springer)
[31] Nesheva D and Levi Z 1997 *Semicond. Sci. Technol.* **12** 1319
[32] Matoussi H, Cumming A W, Murray C B, Bawendi M G and Ober R 1998 *Phys. Rev.* B **58** 7850
[33] Murray C B, Kagan C R and Bawendi M G 2000 *Annu. Rev. Mater. Sci.* **30** 545
[34] Efros Al L and Efros A L 1982 *Fiz. Tekh. Poluprovodn.* **16** 1209
Efros Al L and Efros A L 1982 *Sov. Phys.—Semicond.* **16** 772 (Engl. Transl.)

[35] Norris D J and Bawendi M G 1996 *Phys. Rev.* B **53** 16338
[36] Wang L-W and Zunger A 1996 *Phys. Rev.* B **53** 9579
[37] Rabani E, Hetényi B, Berne B J and Brus R E 1999 *J. Chem. Phys.* **110** 5355
[38] Yu W W, Qu L, Guo W and Peng X 2003 *Chem. Mater.* **15** 2854
[39] Baskoutas S and Terzis A F 2006 *Appl. Phys. Lett.* **99** 013708
[40] Yang C C and Li S 2008 *J. Phys. Chem.* C **112** 2851
[41] Murray C B, Norris D J and Bawendi M G 1993 *J. Am. Chem. Soc.* **115** 8706
[42] Dabbousi B O, Rodriguez-Viejo J, Mikulec F V, Heine J R, Mattoussi H, Ober R, Jensen K F and Bawendi M G 1997 *J. Phys. Chem.* B **101** 9463
[43] Qu L and Peng X 2002 *J. Am. Chem. Soc.* **124** 2049
[44] Madelung O, Rössler U and Schulz M 2006 *Semiconductors* subvolume B (*Landolt-Börnstein—Group III Condensed Matter* vol 41) (Berlin: Springer)
[45] Spanhel L, Haase M, Weller H and Henglein A 1987 *J. Am. Chem. Soc.* **109** 5649
[46] Chestnoy N, Harris T D, Hull R and Brus L E 1986 *J. Phys. Chem.* **90** 3393
[47] Pesika N S, Stebe K J and Searson P S 2003 *J. Phys. Chem.* B **107** 10412
[48] Xie R, Kolb U, Li J, Basché T and Mews A 2005 *J. Am. Chem. Soc.* **127** 7480
[49] Plotnichenko V G, Mityagin Y A and Vodopyanov L K 1977 *Fiz. Tverd. Tela* **19** 2703
Plotnichenko V G, Mityagin Y A and Vodopyanov L K 1977 *Sov. Phys.—Solid State* **19** 1584 (Engl. Transl.)
[50] Hermann C and Yu P Y 1980 *Phys. Rev.* B **21** 3675
[51] Campbell I H and Fauchet P M 1988 *Solid State Commun.* **58** 739
[52] Roy A and Sood A K 1996 *Phys. Rev.* B **53** 12127
[53] Ingale A and Rustagi K C 1998 *Phys. Rev.* B **58** 7197
[54] Gomonnai A V, Azhniuk Yu M, Yukhymchuk V O, Kranjčec M and Lopushansky V V 2003 *Phys. Status Solidi* b **239** 490
[55] Arora A K, Rajalakshmi M, Ravindran T R and Sivasubramanian V 2006 *J. Raman Spectrosc.* **38** 604
[56] Rolo A G and Vasilevskiy M I 2006 *J. Raman Spectrosc.* **38** 618
[57] Azhniuk Y M, Hutych Y I, Lopushansky V V, Raevskaya A E, Stroyuk A L, Kuchmiy S Y, Gomonnai A V and Zahn D R T 2007 *J. Phys.: Conf. Ser.* **79** 012017
[58] Zhou F, Sun Y and Pan J 1988 *J. Lumin.* **40/41** 739
[59] Mlayah A, Brugman A M, Carles R, Renucci J B, Valakh M Y and Pogorelov A V 1994 *Solid State Commun.* **90** 567
[60] Trallero-Giner C, Debernardi A, Cardona M, Menendez-Proupin E and Ekimov A I 1998 *Phys. Rev.* B **57** 4664
[61] Trallero-Giner C 2004 *Phys. Status Solidi* b **241** 572
[62] Azhniuk Y M, Milekhin A G, Gomonnai A V, Lopushansky V V, Yukhymchuk V O, Schulze S, Zenkevich E I and Zahn D R T 2004 *J. Phys.: Condens. Matter* **16** 9069
[63] Dzhagan V M, Valakh M Y, Raevskaya A E, Stroyuk A L, Kuchmiy S Y and Zahn D R T 2007 *J. Phys.: Conf. Ser.* **92** 012045